Summer 8-6-2018

An Analysis of Harmonic Airloads Acting on Helicopter Rotor Blades

Iftekhar A. Riyad
University of New Orleans, iariyad@uno.edu

An Analysis of Harmonic Airloads Acting on Helicopter Rotor Blades

A Thesis

Submitted to the Graduate Faculty of the
University of New Orleans
in partial fulfillment of the
requirements for the degree of

Master of Science
in
Engineering
Mechanical

by

Iftekhar Alam Riyad

B.Sc., Bangladesh University of Engineering and Technology, 2014

August, 2018

DEDICATION

To

My Parents

who have always loved me unconditionally and taught me to work hard for the things that I aspire to achieve

and

My Wife

who has been a constant source of support and encouragement during the challenges of graduate school and life

ACKNOWLEDGMENT

First of all, I thank God almighty for giving me the strength and confidence to carry on this research and for blessing me with many great people who have been my greatest support in both my personal and professional life.

I would like to seize this opportunity to express my deepest regards and gratitude to my supervisor Dr. Uttam K Chakravarty for the continuous support, motivation, and guidance for my Master's study and research. His sense of professionalism, enthusiasm, and immense knowledge helped me to strengthen my skills on professional problem-analyzing, problem-solving, and report-writing. I also want to thank the members of my thesis committee; Dr. Paul J Schilling and Dr. Paul D Herrington for their valuable thoughts and comments on my research.

I would specially like to express my gratitude to Pratik Sarker, whose invaluable knowledge expanded my perspective of this research in many ways. I would like to express my deepest gratitude to Md Mosleh Uddin and M. Shafiqur Rahman who were always there whenever I faced any difficulty about this research. I was lucky enough to have Khairul Habib Pulok and Debabrata Mondal in our lab whose presence made my life at University of New Orleans more enjoyable. Last but not the least; I would like to express my sincere appreciation to my friend Kauser Ahmmed Anik for his valuable insight and advice during the process of generating results.

Table of Contents

Nomenclature

A_n	coefficients of chordwise vorticity distribution
a_0	blade coning angle
a_n	cosine component of blade flapping angle
a	distance between center of twist and center of airfoil
b_n	sine component of blade flapping angle
b	blade semichord
C_L	lift coefficient of the airfoil
C_D	drag coefficient of the airfoil
C_{D0}	average drag coefficient of the airfoil
$C(k)$	lift deficiency function
c	chord length of airfoil
C_T	coefficient of rotor thrust
D	section aerodynamic drag force
d	horizontal distance traveled by rotor hub
h	heaving motion of the airfoil
k	reduced frequency
L	section aerodynamic lift force
M	Mach number
m	number of wake spirals
n	harmonic of rotor speed
Q	number of blades
R	rotor radius
T	rotor thrust

U	freestream velocity
V	forward velocity
V_{tip}	velocity of rotor tip
v	velocity normal to the blade
w	induced velocity at blade due to wake
x	distance along blade chord
z	vertical distance traveled by rotor hub
α	angle of attack
β	blade flapping angle
γ	element of distributed vorticity
δ	angle between rotor disk and relative wind
ξ	distance of element of vorticity from airfoil mid chord
ρ	density of air
Ω	rotor rotational speed
μ	advance ratio
σ	rotor solidity
Γ	blade bound circulation
ψ	azimuth angle of the blade or rotor disk
φ	azimuth of wake measured from downwind position
θ	blade pitch or feathering angle
λ_0	mean inflow coefficient through the rotor disk
λ	inflow coefficient normal to rotor disk
l, η	rotor span parameter
ζ	blade spacing

List of Figures

List of Tables

ABSTRACT

Rotary wing aircrafts in any flight conditions suffer from excessive vibration which makes the passengers feel uncomfortable and causes fatigue failure in the structure. The main sources of vibration are the rotor harmonic airloads which originate primarily from the rapid variation of flow around the blade due to the vortex wake. In this thesis, a mathematical model is developed for rotor blades to compute the harmonic airloads at rotor blades for two flight conditions−vertical takeoff and landing, and forward flight. The sectional lift, drag, and pitching moment are computed at a radial blade station for both flight conditions. The lift at a particular radial station is computed considering trailing and shed vortices and summing over each blade. The results for airloads are obtained by MATLAB after considering zeroth, first, and second harmonics. The calculated results for airloads are compared to the experimental flight-test data.

Keywords: Harmonic airloads, azimuth angle, trailing vortex, shed vortex, vortex wake.

Chapter 1

Introduction

1.1 Motivation

Rotary wing aircrafts are subjected to excessive vibration which makes the passengers uncomfortable and results in fatigue failure in both structure and equipment. There are three basic factors that contribute to the vibration of the helicopter. These three elements are—rotor aerodynamic loading, blade and rotor dynamics, and fuselage dynamics. The primary source of vibration is the aerodynamic loading. One of the most difficult problems faced by the designer of rotary wing aircrafts is the determination of aerodynamic airloads. Among the aerodynamic loading, harmonic airloads are mainly responsible for vibration. For design purpose and cost effectiveness, it is important to understand the harmonic airloads. Rotor harmonic airloads come from two sources— per revolution variation in velocity tangential to the blade and rapid variation in velocity perpendicular to the blade due to vortex wake. To compute the harmonic airloads, the harmonic induced velocity at the rotor blades is computed by the integration of Biot-Savart law over the vortex wake. Tip vortices contribute most to the downwash at the rotor disc. The main objective is to compute the harmonic airloads in hovering and forward flight cases. This is always a challenge to calculate aerodynamic airloads with less computation time without sacrificing accuracy.

1.2 Influence of Airloads on Helicopter Vibration

There are many elements contributing to the vibration of a helicopter. The interaction between the elements determines the degree of complexity required for numerical solution. The elements of vibration can be shown in Fig. 1.1 [1].

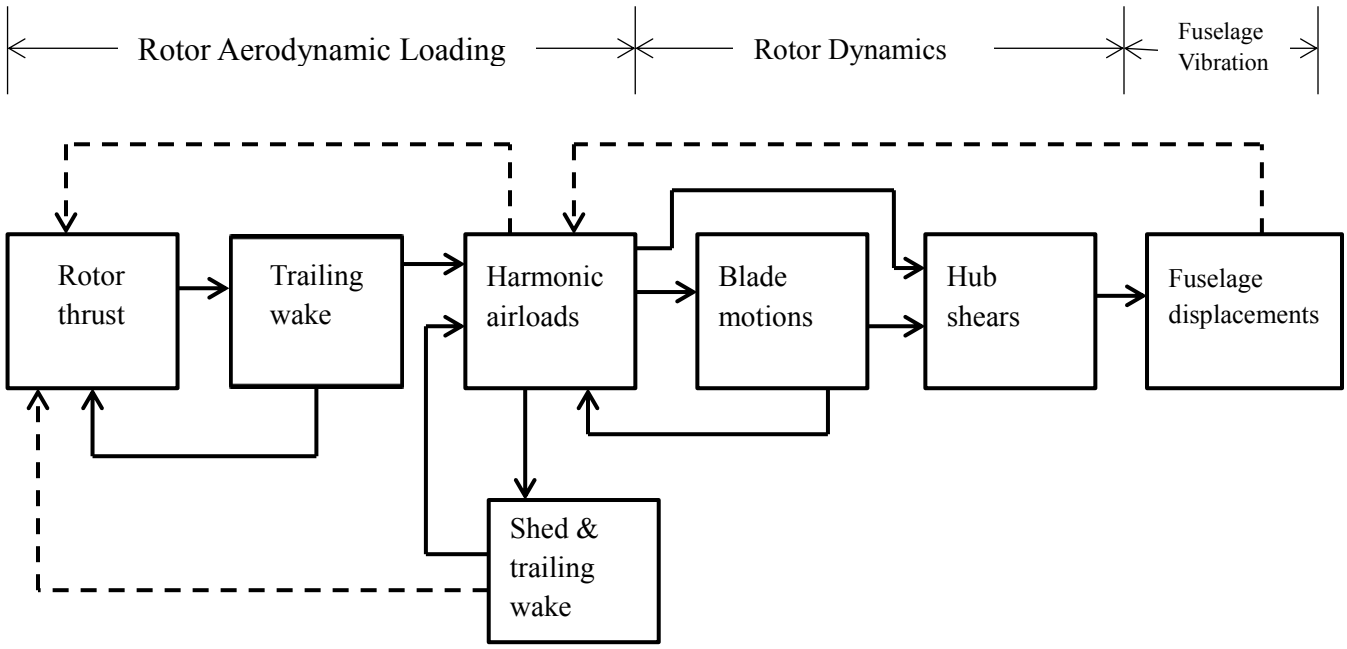

Figure 1.1: Block diagram of elements contributing to helicopter vibration

Research has indicated that the interactions shown by broken lines are not important. The harmonic airloads depend on wake geometry and are the primary source of vibration. Blade motions are coupled with harmonic airloads. Mean rotor thrust, trailing wake, and shed wake are the components that contribute to harmonic airloads. Rotor dynamics and fuselage vibration are also related to harmonic airloads. Blade-vortex interactions (BVI) are responsible for harmonic

airloads. Vortices trailed from one blade interact with next blade which causes the circulation around the wing unsteady. As the rotor blade encounters wake from the preceding blades, substantial time varying loads are produced. Even in steady-state forward flight, the blade loading is periodic in nature. For the computation of airloads, different methods are developed to model the rotor blade vortex in a way so that it becomes mathematically tractable.

1.3 Aerodynamics of Helicopter

Aerodynamics of a helicopter deals with forces and moments necessary to have a controlled and sustainable flight. These forces are called lift and drag. The lift is defined as the component of force acting in a direction perpendicular to the line of flight and drag acts in the direction of flight. Due to the encounter of vortices with rotor blades, the aerodynamics of helicopter is always unsteady in nature.

1.3.1 Unsteady Aerodynamics of Rotor Blades: Helicopter rotor aerodynamics in any flight condition is unsteady in nature because of the rapid change of circulation around the blade. Unlike a fixed-wing aircraft, helicopter rotors experience oscillatory aerodynamic loads even in steady flight condition. Variations in relative speed occur at blade sections when the blade rotates through the azimuth angle. Rotor blades shade helical vortex sheets that remain below the rotor disc which influence the mean inflow through the rotor making the inflow non-uniform. All the aerodynamic loads (lift, drag, and pitching moment) are influenced by the vortices shed from the trailing edge of the blades. For any aerodynamic load calculations, three types of vortices are considered– trailing vortex, shed vortex, and tip vortex. The lift on a blade is due to its bound circulation. Trailing vortices are formed by the spanwise variation of bound circulation and are

parallel to the free stream velocity. Shed vortices are parallel to wing span and are produced due to time variation of bound circulation.

Tip Vortex: Tip vortices results from the rolling up of trailing vortices near the tip of wing and has the major influence on the aerodynamic loads, e.g., lift on a blade is maximum at the blade tip due to the rolled up tip vortices. These vortices are the only concentrated vortices in the helical wake. These tip vortices are formed due to rapid drop in circulation near the blade tip. Most of the trailing vortices outboard of the blade quickly rolls up into concentrated tip vortices. The rest of the trailing wake and shed wake do not roll up until they are far downstream of the flow field. Therefore, tip vortices are the primary source of harmonic airloads. Three types of vortices are illustrated in Fig. 1.2.

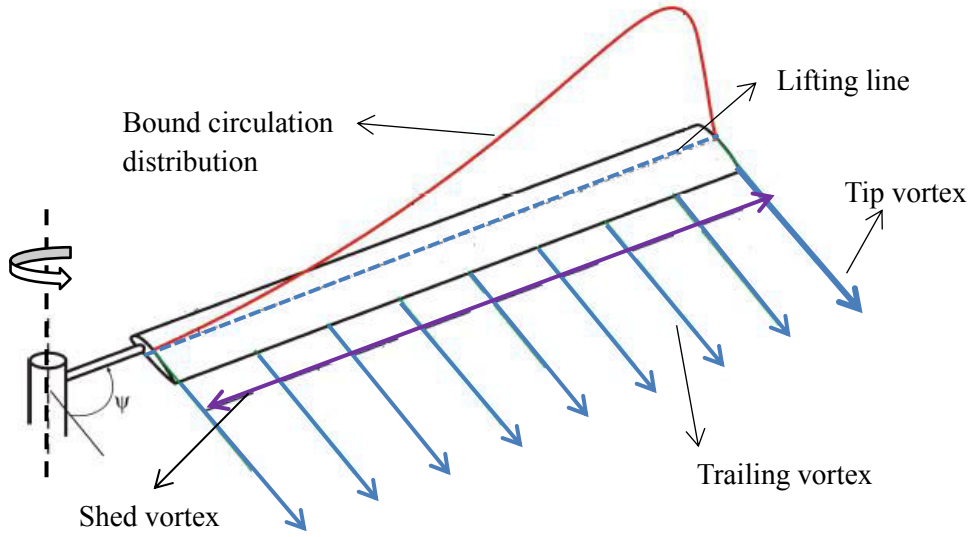

Figure 1.2: Wake vorticity formation in a rotor blade with multiple vortex lines and bound circulation

Harmonic airloads arise from the rapid variation of induced velocity at the rotor blades, radially and azimuthally. This rapid variation is due to the passage of rotor blades close to the concentrated tip vortices in the wake.

1.3.2 Influence of Rotor Wake on Airloads Computation: An airfoil immersed in a free stream experiences a force proportional to the density of surrounding fluid medium, the vortex strength and the freestream velocity. If the wing in a freestream is modeled with a continuous vortex sheet, the total aerodynamic force acting on it can be evaluated as the integral effect of the vortex sheet. In rotary wing aerodynamics, the returning effect of the wake on the neighboring blade can also be modeled with vortex aerodynamics. Since, concentrated tip vortices have the maximum influence on the blade airloads, errors in their location during load computation can lead to wrong induced velocity distribution. Therefore, a rigid wake model is sufficient for trailing and shed vortices but an adequate accurate representation of tip vortices are necessary to compute the airloads accurately. The wake of each blade is assumed to consist of a series of vortex lines, each forming a skewed helix whose geometry is determined by the advance ratio of the helicopter. The computer solution uses numerical integration of Biot-Savart relation over the helical skewed wake. As the integration is done numerically, the wake can be represented by finite straight lines with a varying azimuth of 7.5° to 15°, which is represented in Fig. 1.3. In this thesis, finite line approximation is used for saving a significant amount of computation time. For forward flight case, three spirals of wake can give satisfactory results for airloads calculation. For hovering case, since there is no relative wind, the wake does not move away from the rotor as rapidly as for the forward flight case. Generally, six turns of spirals give satisfactory results and a semi-infinite vortex cylinder is used to represent the tip vortices.

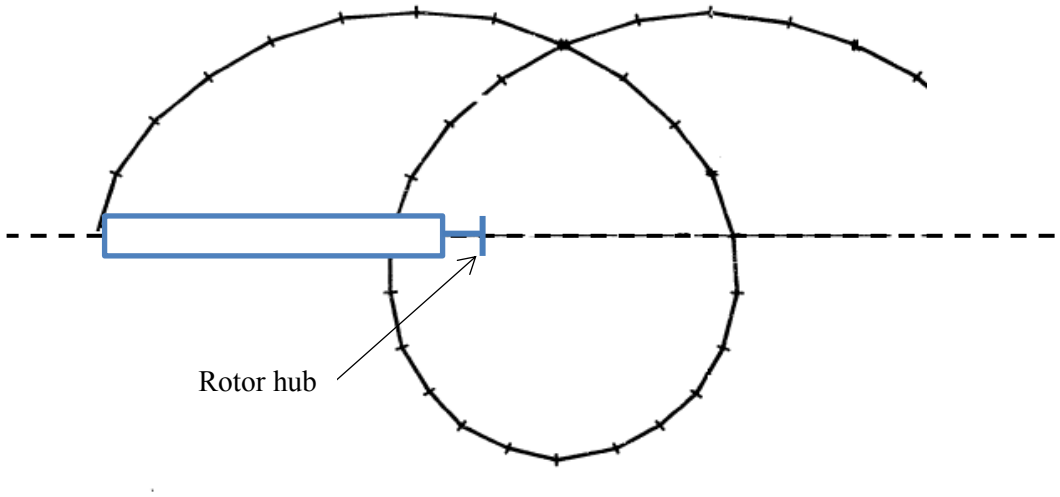

Figure 1.3: Finite straight line approximation of helical vortex wake of a rotor blade

1.4 Review of Literature

Rotary wing aircrafts are subjected to excessive vibration which results in fatigue failure in both the structure and equipment. There are three basic elements that contribute to the vibration of a helicopter. These are—the rotor aerodynamic loadings, rotor dynamics, and fuselage dynamics. Among these three elements, the main source of vibration is the aerodynamic loading, the determination of which is the most difficult problem faced by the rotary wing aircraft designer. Harmonic airloads are mainly responsible for vibration which come from two sources—per revolution variation in velocity tangential to the blade and rapid variation in velocity perpendicular to the blade due to vortex wake. The airloads on a rotor blade also depend on the wake geometry and its distortion during the flight. Harmonic airloads are computed by the integration of trailing and shed wake. The BVI creates noise and vibration in a helicopter and is responsible for harmonic airloads. As the rotary wing encounters the wake generated from the

preceding blades, substantial time-varying loads are produced. For the computation of airloads, different methods [1, 2] were developed to model the rotor blade unsteady aerodynamic problem to calculate the vortex induced airloads. Although extensive work was done in this area for many decades, this is always a challenge to calculate aerodynamic airloads with less computation time and without sacrificing accuracy.

For the fixed-wing aircraft, the influence of the wake distortion can be neglected because the wake is left downstream away from the blade. In case of the rotary wing, the helical vortex wake remains below the rotor disk which influence the mean inflow through the rotor disk making the inflow nonuniform. For the computation of the aerodynamic loadings, three types of vortices are considered−trailing vortex, shed vortex, and tip vortex. Trailing vortices are formed by the spanwise variation of the bound circulation and are parallel to the freestream velocity. Shed vortices are parallel to the wing span and are produced due to the time-variation of bound circulation. Tip vortices are formed by the rolling up of trailing vortices near the tip of the wing and contribute most towards the airloads. The lift on a blade is maximum at the tip due to the tip vortices. Tip vortices are formed due to the rapid drop in the circulation near the blade tip. Most of the trailing vortices outboard of the blade then quickly roll up into concentrated tip vortices. Therefore, tip vortices are the primary source of harmonic airloads. The aerodynamic consideration of a wing can be divided into two parts− the study of the wing section (airfoil) and the modification to the airfoil properties to account for the finite wing [3]. If the wing section in a freestream is modeled with a continuous vortex sheet, the total aerodynamic force acting on it can be evaluated as the integral effect of the vortex sheet. Theodorsen [4] presented the aerodynamic forces acting on an oscillating thin, two-dimensional airfoil which was based on the potential flow and Kutta conditions [3]. Karman, Sears, and Isaacs [5−7] discussed the wake of

vorticity formation by an airfoil and formulated vortex induced airloads equations of an oscillating airfoil. Isaacs [6, 7] considered the practical case where the airfoil was subjected to the variable freestream velocity. The lift and moment equations were developed in the form of the Fourier series considering sinusoidal variation of the freestream velocity and the angle of attack. Loewy [8] considered the aerodynamics of an oscillatory rotary wing airfoil and developed equations for lift and pitching moments with the modified Theodersen's lift-deficiency function. The lift-deficiency function $C(k)$ was modified to include the effects of the number of blades in the rotor, returning wakes, the ratio of oscillatory frequency to rotational frequency, and the inflow ratio. In recent times, the aforementioned theories of two-dimensional airfoil were reviewed and closed form solutions for lift and pitching moment equations were presented in the frequency domain [9−14]. Johnson [15] showed the application of the unsteady airfoil lift and pitching moment equations to three-dimensional rotary wings.

Airloads on a three-dimensional wing are computed by the lifting-line and lifting-surface theory. The computation methods of lifting-line theory were discussed elaborately [16]. In recent times, with a few minor alterations and the use of a modern computer, the lifting-line theory proposed by Prandtl is used to predict the inviscid forces and moments acting on lifting surfaces [17]. The accuracy of the results is as good as that obtained from modern panel codes or computational fluid dynamics (CFD) methods, but at a small fraction of the computational cost. However, Jones [18] showed that the lifting-line theory was adequate to predict the loading distributions in a forward flight, although if a vortex passes very close to the blade, modified lifting-line theory or lifting-surface theory must be used. To achieve the accuracy in the prediction of the blade loadings, it was necessary to consider the chordwise loadings, too. The lifting-surface theory presented by Ashley and Windall [19] emphasized on numerical

approaches to the vortex induced blade loading problem. Landhal [20] applied the numerical lifting-surface theory to linearized thin-wing problem in details and showed comparison with experimental results. The comparison showed that the numerical lifting-surface methods were useful in predicting the airloads accurately. The lifting-surface theory was applied to calculate the lift generated on a rotor blade in forward flight for both compressible and incompressible flows [21]. The method utilized the concept of the linearized acceleration potential originally developed by Kussner [22] and calculations were demonstrated in terms of the lift distribution on a single and double bladed rotor. Johnson [23] developed a practical procedure for the use of the lifting-surface theory to calculate the airloads induced on a helicopter rotor blade by a nearby tip vortex. Planar lifting-surface theory was applied to the model problem of an infinite aspect ratio of the wing encountering an infinite vortex at an arbitrary angle with the wing. The solution of the problem required the development of the general aerodynamic kernel function developed and modified by Watkins and others [24, 25]. Johnson showed that the use of the lifting surface solution [18] was necessary to obtain accurate loading prediction for the case involving the tip vortex passing close to the blade.

One of the earliest attempts to compute the induced velocity field at the rotor flow was presented by Drees [26] primarily for the purpose of performance estimation. Miller [27] presented a theoretical approach of determining blade harmonic airloads in both hovering and forward flights. The first step of airloads calculation was to compute the vortex induced downwash at the rotor disk at a particular spanwise distance. Biot-Savart induction law [3] was used to calculate the downwash at a particular spanwise station. Miller [27] presented the equations to compute the downwash for the trailing and shed wakes using the Biot-Savart law [28]. Integration of these equations gave the total downwash at a particular blade station. Mean

inflow through the rotor disk was then calculated which was used to compute the lift force on the blade section. Ghareeb [29] programmed the procedure of the lift calculation described in an IBM 7090 computer at MIT. Later, Scully [30, 31] discussed the various methods of calculating the airloads on a helicopter rotor in steady, forward flight for the purpose of achieving faster solution time for a given level of accuracy. Widnall [32] discussed the stability of a helical vortex filament of finite core size and concluded that the vortex was unstable to small sinusoidal displacements of the filament. Scully [33] and Landgrebe [34] presented the methods to predict the rotor blade wake geometry. The airloads solution used numerical integration of the Biot-Savart relation [27] over the helical skewed wake. As the integration was done numerically, the wake was represented by finite straight lines [35, 36] with a varying azimuth of 7.5° to 15°. The airloads calculation using the Biot-Savart law [27] with the lifting-line approximation gives almost accurate results for lower harmonics. In recent times, the application of numerical panel methods [37−44] and inviscid CFD methods [45−48] are popular for the fast computation of the airloads using CAMRAD II software designed specially for the rotary wing.

1.5 Research Objective

The objective of this thesis is to present a mathematical model to compute the harmonic airloads. A simplified mathematical model is developed to make the airloads expressions mathematically tractable. For forward flight case, assuming a harmonic circulation and semirigid trailing wake, the numerical integration of the Biot-Savart relation [28] is carried out over the helical vortex to find the induced downwash at a radial station. Harmonic analysis is carried out on the downwash velocity to compute the mean inflow through the rotor disk. By computing the inflow, the lift at a particular spanwise station is calculated with varying azimuth angle. For both flight conditions, three spirals of the vortex are considered for the airloads calculation. Results

for airloads are obtained by considering the zeroth, first, and second harmonics only. The pitching moment and sectional drag are also calculated along with lift force and all the results are expressed in nondimensionalized form. For the airloads computation, the parameters of the UH-60 helicopter rotor blade are used. All the computations are done in MATLAB.

All the numerical calculations and plots have been done in MATLAB 2015a. The Results obtained for lift are then compared to the experimental results of full scale flight tests.

Chapter 2

Theoretical Context on Rotor Blade Aerodynamics

2.1 Classical Theories of Aerodynamics

Aerodynamics deals with forces and moments necessary to have a controlled and sustainable flight for any aircraft. These forces are called lift and drag. The lift is defined as the component of force acting in a direction perpendicular to the line of flight which must be greater than the force of gravity in order to ascend the aircraft. The drag acts in the direction of flight, which is the resistance felt by the aircraft against the flow of air. The lift and drag equations for an airfoil section are given as [3]:

$$L = \frac{1}{2}\rho U^2 c C_L \tag{1}$$

$$D = \frac{1}{2}\rho U^2 c C_D \tag{2}$$

The lift generated on an airfoil can also be expressed as a function of its bound circulation. Among the classical theories of aerodynamics, Kutta condition [3] gives the circulation nature around the airfoil which states that a body with a sharp trailing edge which is moving through a fluid will create about itself a circulation of sufficient strength to hold the rear stagnation point at the trailing edge i.e., the vortex will be produced at the trailing edge only. Kelvin's circulation theory [45] states that the circulation around the airfoil is equal and opposite of the circulation around the starting vortex. The well-known Kutta-Joukowski theorem [3] relates the lift generated by an airfoil to the airfoil speed, fluid density, and the circulation around the airfoil. According to this theory, the lift per unit length is given by,

$$L = \rho U \Gamma \tag{3}$$

The theorems discussed apply only for the steady-state condition. When the flow velocity around the airfoil increases (which is the case for all aircrafts) i.e., the Reynolds number Re increases, the flow becomes unsteady in nature. In order to calculate the unsteady lift, drag and pitching moment, the magnitude of induced velocity by the trailing vortices around the airfoil is to be known. The conservation of vorticity for a finite wing requires that there will be trailing and shed vorticities in the wake behind the wing. The trailing vorticity is parallel to the freestream velocity and is produced due to the spanwise variation of bound circulation. The shed vorticity is parallel to the blade span and is produced due to the time variation of bound circulation. The resultant vortex behind the wing is the combination of trailed and shed vorticity.

In this thesis, the airloads at a spanwise station of a blade will be calculated using the Biot-Savart law. The concept of vortex filament is necessary for the application of this law. A

vortex filament can be a curved line which extends from the trailing edge of the blade. A portion of vortex filament is shown in Fig. 3.1 [3].

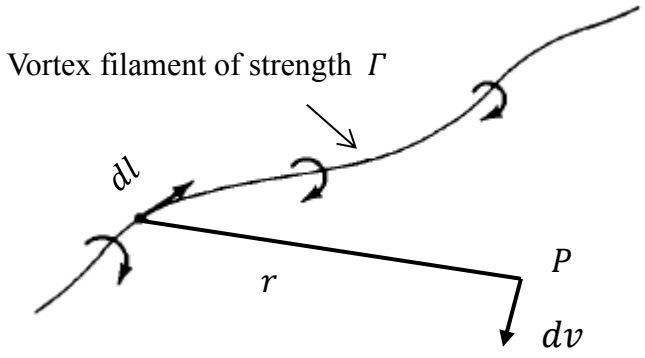

Figure 2.1: Induction by vortex filament at a point near the filament

The filament induces a flow field in the surrounding space. The strength of vortex filament is assumed as Γ. Let us consider a small segment of the filament dl, as shown in Fig. 2.1. The radius vector from dl to an arbitrary point P in space is r. The segment dl induces velocity dv at P which is expressed as:

$$dv = \frac{\Gamma}{4\pi}\frac{dl \times r}{r^3} \tag{4}$$

Equation (4) is known as Biot-Savart law and is one of the fundamental equations in the theory of inviscid incompressible flow. Helmholtz [3] was the first to make use of the vortex filament concept in the analysis of inviscid, incompressible flow and to calculate the airloads. The Helmholtz theorem states that:

1. The strength of a vortex filament is constant along its length.

2. A vortex filament cannot end in a fluid; it must extend to the boundaries of the fluid or form a closed path.

These theorems are the basics of the theory of lift distribution along the span of a finite blade.

The aerodynamic study of a wing can be separated into two categories−the study of wing section (airfoil), and the study of three-dimensional wing. The first practical theory for predicting the aerodynamic properties of a finite wing was developed by Prandtl [3, 16]. The utility of Prandtl's theory is still in use today for preliminary calculations of wing characteristics. This lifting-line theory is the basis of modern numerical methods for calculating the blade loadings. The lifting-line approach assumes a straight line along the span of a wing and calculates the lift along this line only. This method does not necessarily give the accurate prediction of airloads but gives a preliminary idea about the airloads.

2.2 Two-Dimensional Aerodynamics of Airfoil

Since the aerodynamic environment of the rotor blade in hovering or forward flight is unsteady, lifting-line theory requires an analysis of the unsteady aerodynamic environment of a two-dimensional airfoil. Considering the problem of a two-dimensional airfoil undergoing unsteady motion in a uniform freestream, the airfoil and its wake are represented by thin surfaces of vorticity parallel to the freestream velocity given in Fig. 2.2 [16]. The shed vorticity in unsteady aerodynamic environment are modeled by planar sheets of vorticity. An airfoil of chord $2b$ is in a uniform freestream velocity U. Since the bound circulation of the section varies with time, there is shed vorticity in the wake downstream of the airfoil. The vorticity strength on the airfoil is γ_b and the wake is γ_w. The blade motion is described by a heaving motion h (positive

downward) and a pitch angle α about an axis at $x = ab$ (positive for nose upward). The aerodynamic pitch moment is evaluated about the axis at $x = ab$.

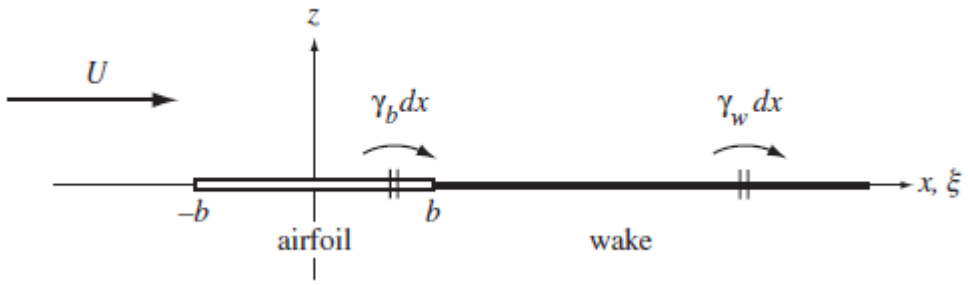

Figure 2.2: Unsteady thin airfoil model of a two-dimensional wing and its wake

The lift and the pitching moment of a two-dimensional airfoil are expressed as [15]:

$$L = \pi\rho b^2\left(\ddot{h} + U\dot{\alpha} - ba\ddot{\alpha}\right) + 2\pi\rho Ubc\left(\dot{h} + U\alpha + \left(\frac{1}{2} - a\right)\dot{\alpha}\right) \tag{5}$$

$$M = \pi\rho b^2\left[ab(\dot{h} + U\alpha) - Ub\frac{1}{2}\dot{\alpha} - b^2\left(\frac{1}{8} + a^2\right)\ddot{\alpha}\right] + 2\pi\rho Ub^2\left(a + \frac{1}{2}\right)C(k)[(\dot{h} + U\alpha) + b(\frac{1}{2} - a)\dot{\alpha}] \tag{6}$$

For the complete analysis of the airloads of a wing, it is necessary to consider the three-dimensional wing. A finite blade is a three-dimensional body and the flow around it is also three-dimensional; i.e., there is a component of flow in the spanwise direction. The blade experiences lift due to the existence of a high pressure on the bottom surface and a low pressure on the top surface of the blade. The net imbalance of the pressure distribution creates the lift and the

pressure imbalance. The flow near the wing tip tends to curl around the tips, being forced from the high pressure region just underneath the tips to the low-pressure region on top. As a result, on the top surface of the wing, there is generally a spanwise component of flow from the tip toward the wing root, causing the streamlines over the top surface to bend toward the root. Similarly, on the bottom surface of the wing, there is a span wise component of flow from the root toward the tip, causing the streamlines over the bottom surface to bend toward the tip and tip-vortex is formed. The tendency of the flow to leak around the blade tips has another important effect on the aerodynamics of the blade. This flow causes a circulatory motion which trails downstream of the blade; i.e., trailing vortices are created at the trailing edge of blade sections. These trailing vortices downstream of the wing induce a small downward component of air velocity in the neighbourhood of the blade itself. These vortices tend to drag the surrounding air around with them, and this secondary movement induces a small velocity component in the downward direction at the wing. This downward component is called downwash w. The downwash combines with the freestream velocity U and has its effect on the lift and thrust generation on the blade.

Chapter 3

Mathematical Model for Blade Airload Calculation

3.1 Two-Dimensional Vorticity Distribution

The problem of calculating the unsteady loads on a three-dimensional wing can be divided into two parts—an inner problem involving the aerodynamic behavior of a two-dimensional airfoil, and an outer problem involving the calculation of the velocity induced by the rotor vortex wake at the blade section [16]. Johnson [16, 49] discussed the unsteady two-dimensional aerodynamic model for a rotary wing. The vorticity distribution induced by a vortex of constant strength measured from the midchord position of the airfoil is expressed as [5]:

$$\gamma(x) = \frac{1}{\pi}\frac{\Gamma}{\xi - x}\sqrt{\frac{1-x}{1+x}}\sqrt{\frac{\xi+1}{\xi-1}} \tag{7}$$

where x is the distance along the blade chord and $-1 \le x \le 1$, ξ is the distance of the vortex from the midchord, Γ is the circulation strength of an element of vorticity. The chordwise vorticity can also be represented by the following series [50]:

$$\gamma(x) = A_0 \tan\frac{\theta}{2} + \sum_{n=1}^{\infty} A_n \sin n\theta \tag{8}$$

The flow normal to the blade at a chordwise station x can be written as [1]:

$$v(x) = \frac{A_0}{2} + \sum_{n=1}^{\infty} \frac{A_n}{2}\cos n\theta \tag{9}$$

where A_n is the Fourier coefficient of chordwise vorticity distribution and n is the number of harmonics [50]. A two-dimensional lifting-surface theory considering the chordwise vorticity was developed [1, 35] and shown that the lift expression could be given in terms of the coefficients of chordwise vorticity A_n as:

$$L = \pi\rho b\left[\frac{1}{2}\frac{\partial}{\partial t}\left(A_0 - \frac{1}{2}A_2\right)b + \frac{\partial}{\partial t}\left(A_0 + \frac{1}{2}A_1\right)b + V\left(A_0 + \frac{1}{2}A_1\right)\right] \tag{10}$$

3.2 Three-Dimensional Rotor Induced Downwash

Three-dimensional system of the rotor wake is completed by trailing vortex lines generated by the blade. Shed vortices generate as a result of time variation of circulation around the blade. Among the trailing vortices, tip vortex has the highest influence on the blade loading. The three-dimensional model for the airloads calculation consists of the trailing and shed vortex lines generated by the changes in circulation along the blade span shown in Fig. 3.1. The nature of the wake is semirigid, i.e., every element of the vorticity is assumed to retain the instantaneous vertical velocity imparted to it at the moment it is trailed or shed. This assumption establishes a spiral wake descending at every spanwise station with a constant velocity in time but permits different vertical velocities azimuthwise. Since the induced velocity at the blade span is determined mainly by the first few spirals, this assumption is considered to be valid [27]. The relationship required to compute the downwash at a spanwise station of rotor blade is developed below. Numerical integration of the Biot-Savart relation [51] is used to calculate the total downwash at the blade station for a three-dimensional rotor, operating at an advance ratio μ.

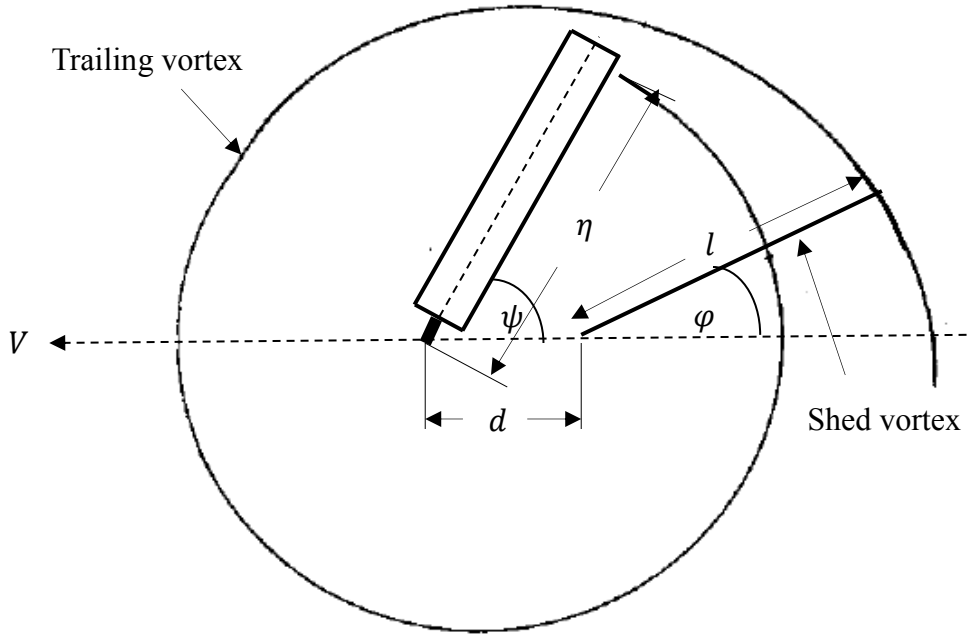

Figure 3.1: Wake geometry showing trailing and shed vortex wake

From Fig. 3.1, the element of vorticity is generated from the trailing edge of the blade at a spanwise station l from the center of the rotor hub when the blade is at an angle φ. The vertical component of downwash, dw_1 induced at another spanwise station η and chordwise station x by this wake element at the azimuth angle, ψ is given [1] as:

$$dw_1 = \frac{\Gamma}{4\pi R} \quad \frac{ds_2 A_1 - ds_1 A_2}{\left({A_1}^2 + {A_2}^2 + {A_3}^2\right)^{\frac{3}{2}}} \tag{11}$$

$$ds_1 = \mu d\varphi \cos\varphi \tag{12}$$

$$ds_2 = \mu d\varphi \sin\varphi + l d\varphi \tag{13}$$

$$A_1 = l + d\cos\varphi - \eta\cos(\psi - \varphi) - x\sin(\psi - \varphi) \tag{14}$$

$$A_2 = d\sin\varphi + \eta\sin(\psi - \varphi) - x\cos(\psi - \varphi) \tag{15}$$

$$A_3 = -z \tag{16}$$

$$d = [(2\pi m + \psi) - \varphi + \zeta]\mu \tag{17}$$

$$z = [(2\pi m + \psi) - \varphi + \zeta]\lambda + z_o(\eta) - z_o(l) \tag{18}$$

where d is the distance travelled by rotor hub during the time, $t = (\psi - \varphi)/\Omega$, and z is the vertical distance of element of vorticity below the blade. z_o is the steady-state displacement of the blade out of the tip-path plane (TPP). For a rigid wake, $z_o(\eta) - z_o(l) = a_o(\eta - l)$. ζ is the spacing of the blades and for a four-bladed rotor, ζ has values 0, $\pi/2$, π, and $3\pi/2$. The downwash for a single trailing vortex and a single blade is calculated by integrating Eq. (11) over the number of the spirals considered. The downwash due to the shed vorticity [27] is expressed as:

$$dw_2 = -\frac{\Gamma}{4\pi R}\frac{d\Gamma}{d\varphi}\,d\varphi\;\frac{A_2 dl}{\left({A_1}^2 + {A_2}^2 + {A_3}^2\right)^{\frac{3}{2}}} \tag{19}$$

To find the total downwash w_2, Eq. (19) is integrated with respect to l over each finite interval before integration with respect to φ. The summation of downwash due to trailing and shed vorticity is:

$$w = w_1 + w_2 \tag{20}$$

The bound circulation induced on the blade at a particular spanwise station and the corresponding lift force are given [1] as:

$$\Gamma_b = -2\pi bw \tag{21}$$

$$L(\psi, \eta) = -2\pi\rho bwU = \rho\Gamma_b U \tag{22}$$

Equation (22) gives the lift equation at a particular spanwise station and a particular azimuth angle. Total lift at any spanwise station can be calculated using Eq. (22) after summing over all the blades.

3.3 Three-Dimensional Airloads Solution

3.3.1 Hovering Flight Condition: Three-dimensional downwash calculation for hovering or vertical flight is mainly based on uniform downwash. For the hovering case, Eq. (11) becomes:

$$dw_1 = \frac{\Gamma}{4\pi R} \quad \frac{[1 - \eta\cos(\psi - \varphi)]d\varphi}{[1^2 + \eta^2 + z^2 - 2\eta\cos(\psi - \varphi)]^{\frac{3}{2}}} \tag{23}$$

Now, replacing the spiral of the trailing vorticity of strength, Γ by a vortex cylinder, the distribution of vorticity along z axis is given by:

$$\frac{d\Gamma}{dz} = \frac{\Gamma Q}{2\pi\lambda_O} \tag{24}$$

where λ_O is the mean inflow normal to the rotor disk. The downwash velocity due to trailing vortices is obtained by integrating over the complete wake as:

$$w_1 = \frac{Q}{8\pi^2 \lambda_O R} \int_0^{2\pi} \frac{\Gamma[1 - \eta \cos(\psi - \varphi)]}{[1^2 + \eta^2 - 2\eta \cos(\psi - \varphi)]} d\varphi \tag{25}$$

Since, $\lambda_O = w/\Omega R$ for hovering flight, the constant circulation strength is expressed by:

$$\Gamma = \frac{4\pi {\lambda_O}^2 \Omega R^2}{Q} \tag{26}$$

From definition, the coefficient of thrust is:

$$C_T = \frac{T}{\rho \pi R^4 \Omega^2} \tag{27}$$

and

$$\lambda_O = \sqrt{\frac{C_T}{2}} \tag{28}$$

The lift depends on the bound circulation around the blade section. The harmonic variation of bound circulation $\Gamma_n(\varphi)$ is given as follows:

$$\Gamma_n(\varphi) = \Gamma_{ns} \sin n\varphi + \Gamma_{nc} \cos n\varphi \tag{29}$$

From Eq. (5), the downwash due to trailing vorticity is:

$$w_1 = \frac{Q}{8\pi^2\lambda_O R}\int_0^{2\pi m} \Gamma_n(\varphi)\frac{[1-\eta\cos(\psi-\varphi)]}{[1^2+\eta^2-2\eta\cos(\psi-\varphi)]}d\varphi \tag{30}$$

For the complete solution of downwash, the effect of shed vorticity is to be considered and for hovering case, Eq. (19) becomes:

$$w_2 = \frac{Q}{8\pi^2\lambda_O R}\int_0^{2\pi m}\int_0^{\eta}\frac{d\Gamma}{d\varphi}\,d\varphi\,[\frac{1}{\eta}\sin(\psi-\varphi)+\frac{l}{\eta^2}\sin 2(\psi-\varphi)]dl$$
$$+\frac{Q}{8\pi^2\lambda_O R}\int_0^{2\pi m}\int_{\eta}^{1}\frac{d\Gamma}{d\varphi}\,d\varphi\,[\frac{\eta}{l^2}\sin(\psi-\varphi)+\frac{\eta^2}{l^3}\sin 2(\psi-\varphi)]dl \tag{31}$$

which can be reduced to the form below given in Eq. (32), after substituting $\Gamma_n(\varphi) = \Gamma_{ns}\sin n\varphi + \Gamma_{nc}\cos n\varphi$ and integrating over φ and l.

$$w_2 = \frac{Q}{8\pi^2\lambda_O R}[\Gamma_{ns}(2-\eta^n)\pi\sin n\psi + \Gamma_{nc}(2-\eta^n)\pi\cos n\psi] \tag{32}$$

After calculating w_1 and w_2 for a spanwise station, total downwash w and the corresponding lift are calculated using Eqs. (20) and (22) after summing over all blades and all the trailing and shed vortices for hovering flight condition.

3.3.2 Forward Flight Condition: Rotor blades in forward flight are subject to variable velocities and airloads are maximum on the advancing side of blades and minimum on the retreating side. Using the downwash theory [27, 28] and considering the blade to be in flapping

equilibrium, the blade loadings for an advance ratio are calculated. Like in hovering case, the forward flight case also consists of trailing and shed wakes. The downwash Eq. (23) due to the trailing wake takes the form for the forward flight case as:

$$dw_1 = \frac{\Gamma(\varphi)}{4\pi R} \frac{[l + d\cos\varphi - \eta\cos(\psi - \varphi)]ld\varphi}{[l^2 + d^2 + \eta^2 + z^2 - 2\eta l\cos(\psi - \varphi) + 2ld\cos\varphi - 2\eta d\cos\psi]} \quad (33)$$

Equation (33) is simplified to the case of a lifting-line theory for the simplicity of calculations where the chordwise station x is neglected. The time variation of circulation gives rise to shed vorticity and must be considered for the computation of the airloads. The downwash at the blade due to the shed wake can be represented as [28]:

$$dw_2 = -\frac{1}{4\pi R}\frac{d\Gamma(\varphi)}{d\varphi}\frac{[\eta\sin(\psi - \varphi) - x\cos(\psi - \varphi) + d\sin\varphi]dl}{[p^2 + x^2 - 2xl\sin(\psi - \varphi) - 2xd]^3}\, d\varphi \quad (34)$$

where

$$p^2 = l^2 + d^2 + \eta^2 + z^2 - 2\eta l\, cos(\psi - \varphi) + 2ld\, cos - 2\eta d\, cos\,\psi \quad (35)$$

One important difference between Eqs. (33) and (34) is the presence of chordwise station x in Eq. (34). However, if chordwise station is ignored for the computation of the shed wake, the lifting-line theory must be applied and Eq. (34) takes the form as:

$$dw_2$$

$$= -\frac{1}{4\pi R}\left[\frac{\eta\, sin(\psi-\varphi)+d\, sin\,\varphi}{z^2+[\eta\sin(\psi-\varphi)+d\sin\varphi]^2}\left\{\frac{l+d\,cos\,\varphi-\eta\,cos(\psi-\varphi)}{\sqrt{l^2+\eta^2+z^2+d^2-2\eta\,cos(\psi-\varphi)+2d(l\,cos\,\varphi-\eta\,cos\,\psi)}}\right.\right.$$

$$\left.\left.-\frac{d\,cos\,\varphi-\eta\,cos(\psi-\varphi)}{\sqrt{d^2+\eta^2+z^2-2\eta d\,cos\,\psi}}\right\}\right]\frac{d\Gamma(\varphi)}{d\varphi}d\varphi \tag{36}$$

The total downwash due to shed wake can be obtained by the numerical integration of Eq. (36).

After the numerical integration for downwash due to the trailing and shed wakes from Eqs. (33) and (36) for forward flight case, the harmonic analysis of w_1 and w_2 are done [28, 29]. Harmonic analyses are carried out using the following expressions:

$$\frac{w_1(\psi)}{\Omega R} = P_{0_{jk}} + \sum_{i=1}^{n}\left[P_{i_{jk}}\,cos(i\psi) + Q_{i_{jk}}\,sin(i\psi)\right] \tag{37}$$

$$\frac{w_2(\psi)}{\Omega R} = A_{0_{jk}} + \sum_{i=1}^{n}\left[A_{i_{jk}}\,cos(i\psi) + B_{i_{jk}}\,sin(i\psi)\right] \tag{38}$$

where the subscripts i, j, and k correspond to the number of harmonics considered, the spanwise distance where downwash is calculated, and the spanwise distance of the trailing or shed wake from rotor hub, respectively. For zeroth harmonic, there is no sine component, so only cosine components are considered in the calculation of airloads. For the other harmonics, P and Q from Eq. (37) refers to cosine and sine components of downwash due to the trailing wake, respectively. For the shed wake, A and B refer to cosine and sine components of the downwash, respectively. After calculating the components, the load coefficients, i.e., the inflow coefficients

through the rotor disk due to the trailing wake are calculated using the following formula [28, 29]:

$$\lambda_{0_j} = \frac{b}{2R}\sum_{t=1}^{m}\left[(\eta\theta_t - \lambda_0)\left(P_{0_{jt}} - P_{0_{jt-1}}\right)\right] - \mu\tan\delta \tag{39}$$

$$\lambda_{ic_j} = \frac{b}{2R}\sum_{t=1}^{m}\left[(\eta\theta_t - \lambda_0)\left(P_{i_{jt}} - P_{i_{jt-1}}\right)\right] \tag{40}$$

$$\lambda_{is_j} = \frac{b}{2R}\sum_{t=1}^{m}\left[(\eta\theta_t - \lambda_0)\left(Q_{i_{jt}} - Q_{i_{jt-1}}\right)\right] \tag{41}$$

The load coefficients due to shed wake are calculated by the following expression [29]:

$$\lambda_j = \frac{b}{2R}\sum_{t=1}^{m}\left[(\eta\theta_t - \lambda_0)\left(A_{i_{jt}} - A_{i_{jt-1}}\right)\right] - \mu\tan\delta \tag{42}$$

The lift at any spanwise station is dependent on the bound circulation Γ_n. For the convenience of calculation, the bound circulation is nondimensionalized as:

$$\gamma_n = \frac{\Gamma_n}{2\pi b\Omega R} \tag{43}$$

The inflow coefficient λ and bound circulation γ can be related to a particular spanwise station η as follows [28]:

$$\gamma_0 = \eta\theta - \lambda_0 + \frac{\mu}{2}a_1 \tag{44}$$

$$\gamma_{1s} = \mu\theta - \lambda_{1s} - a_1\eta + \frac{\mu}{2}b_2 \tag{45}$$

$$\gamma_{1c} = -\lambda_{1c} + b_1\eta - a_0\mu + \frac{\mu}{2}a_2 \tag{46}$$

$$\gamma_{ns} = -\lambda_{ns} - n\,\eta a_n + \frac{\mu}{2}(b_{n+1} + b_{n-1}) \tag{47}$$

$$\gamma_{nc} = -\lambda_{nc} + n\,\eta b_n + \frac{\mu}{2}(a_{n+1} + a_{n-1}) \tag{48}$$

where $a_0, a_n,$ and b_n are the blade flapping coefficients obtained from the following blade flapping equilibrium equation [1]:

$$I\ddot{\beta} + I\Omega^2\beta = \int_0^1 \frac{1}{2}\rho c C_L(\Omega\eta + U\sin\psi)\eta\, d\eta \tag{49}$$

The harmonic variations of blade pitching angle considering second harmonics are calculated using the following expressions:

$$\theta = \theta_0 + \theta_{1c}\cos\psi + \theta_{1s}\sin\psi + \theta_{2c}\,cos(2\psi) + \theta_{2s}\,sin(2\psi) \tag{50}$$

Now, using the lifting-line theory, the sine and the cosine components of airloads for a particular harmonic number at a station η on the blade are expressed as:

$$L_{nc} = 2\pi\rho b\Omega^2 R^2 \left[\eta\, \gamma_{nc} + \frac{\mu}{2}\{\gamma_{(n+1)_s} - \gamma_{(n-1)_s}\}\right] \tag{51}$$

$$L_{ns} = 2\pi\rho b\Omega^2 R^2 \left[\eta\, \gamma_{ns} + \frac{\mu}{2}\{\gamma_{(n-1)_c} - \gamma_{(n+1)_c}\}\right] \tag{52}$$

Total lift of a section at a spanwise station η with varying azimuth angle ψ after extracting zeroth, first, and second harmonics can be expressed as [29]:

$$\begin{aligned} L_j(\psi) = 2\pi\rho b\Omega^2 R^2 \Big[& \left(\eta_j + \mu\sin\psi\right)\lambda_j(\psi) - \eta_j\lambda_{0_j} - \frac{\mu}{2}\lambda_{1s_j} \\ & - \left(\eta_j\lambda_{1c_j} + \frac{\mu}{2}\lambda_{2s_j}\right)\cos\psi - \left(\eta_j\lambda_{1s_j} + \mu\lambda_{0_j} - \frac{\mu}{2}\lambda_{2c_j}\right)\sin\psi \\ & - \left(\eta_j\lambda_{2c_j} - \frac{\mu}{2}\lambda_{1s_j} + \frac{\mu}{2}\lambda_{3s_j}\right)\cos(2\psi) \\ & - \left(\eta_j\lambda_{2s_j} + \frac{\mu}{2}\lambda_{1c_j} - \frac{\mu}{2}\lambda_{3c_j}\right)\sin(2\psi)\Big] \end{aligned} \tag{53}$$

The procedures to calculate lift at a spanwise station can be summarized as follows:

1. Assume a mean inflow λ_0 and calculate sine and cosine components of downwash $w_1$and w_2 from Eqs. (33) and (36), respectively.

2. Harmonic analysis is carried out to calculate the harmonic airloads coefficients.

3. Calculate λ_0 using Eq. (39) and use this value in step 1 to calculate downwash and in step 2 to calculate the harmonic airloads coefficients.

4. Calculate the sine and cosine components of inflow for different harmonics form Eqs. (39) −(42).

5. Calculate sine and cosine components of lift using Eqs. (51) and (52) and total lift by extracting up to second harmonics from Eq. (53).

3.4 Determination of Sectional Drag

The sectional drag of the blade is dependent on the angle of attack and the Mach number. Time-varying angle of attack, three-dimensional flow effects at the blade tip, tangential airspeed at radial station, and airspeed perpendicular to no feathering plane (NFP) are considered for unsteady aerodynamics of helicopter. There are two components of the drag– viscous drag and vortex induced drag. The total drag of the sectional profile is:

$$D_T = D_0 + D_i = \frac{1}{2}\rho\mu^2\Omega^2R^2c\ C_{Do} + \frac{1}{2}\rho c C_L U_T U_P \tag{54}$$

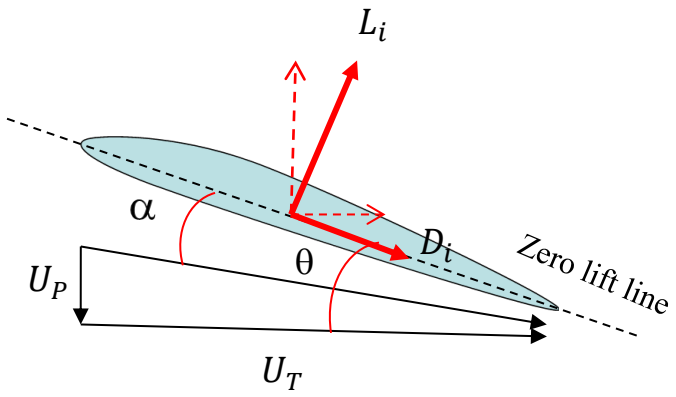

Figure 3.2: Induced drag on on airfoil section

Now, the tangential airspeed U_T and the perpendicular airspeed U_P can be expressed as [16]:

$$U_T = \Omega\eta + \Omega R\mu \sin\psi \tag{55}$$

$$U_P = \Omega R\lambda + \eta\dot{\beta} + \beta\Omega R\mu\cos\psi \tag{56}$$

Blade flapping angle $\beta(\psi)$ can be found from the blade flapping equilibrium Eq. (49). The general solution of Eq. (49) is given as:

$$\beta(\psi) = a_0 + a_1\cos\psi + b_1\sin\psi + a_2\cos(2\psi) + b_2\sin(2\psi) \tag{57}$$

The values of the coefficients are taken from literature survey for the calculation of sectional drag. After determining all the dependent variables, sectional drag is determined using Eq. (54). The values for flapping and pitching coefficients [52−56] of the UH-60 helicopter are given in Table 1.

Table 1: Flapping and Pitching Coefficients for UH-60 Helicopter

Parameters	Value	Parameters	Value
θ_0	13.51°	a_0	6.9°
θ_{1c}	2.47°	a_1	−5.9°
θ_{1s}	−8.99°	b_1	−2.2°
θ_{2c}	1.8°	a_2	−4.67°
θ_{2s}	−6.25°	b_2	−1.7°

3.5 Determination of Pitching Moment

According to the Theodorsen's theory [4] of a thin, two-dimensional airfoil undergoing unsteady motion in an incompressible flow, the pitching moment equation is given as [15]:

$$M = \pi\rho b^2\left[ab\ddot{h} - Ub\left(\frac{1}{2}-a\right)\dot{\alpha} - b^2\left(\frac{1}{8}+a^2\right)\ddot{\alpha}\right] + 2\pi\rho U b^2\left(a+\frac{1}{2}\right)C(k)\left[\dot{h}+U\alpha+b\left(\frac{1}{2}-a\right)\dot{\alpha}\right] \quad (58)$$

The airfoil has the heaving displacement h and the angle of attack α. $C(k)$ is the Theodorsen lift deficiency function. The normal velocity due to the airfoil motion is given as:

$$w_a = -\left(\dot{h}+U\alpha\right) - \dot{\alpha}(x-ab) \quad (59)$$

Through Eq. (59), the airfoil motion enters into the rotary wing problem. The boundary condition of the unsteady airfoil theory is that there is no flow through the wing surface [16]. These boundary conditions depend on the quantities $(\dot{h}+U\theta)$ and $\dot{\theta}$ and the solution of this linear problem also depends on these two quantities. So, Eq. (58) takes the form:

$$M = \pi\rho b^2\left[ab(\dot{h}+U\alpha) - Ub\frac{1}{2}\dot{\alpha} - b^2\left(\frac{1}{8}+a^2\right)\ddot{\alpha}\right] + 2\pi\rho U b^2\left(a+\frac{1}{2}\right)C(k)[(\dot{h}+U\alpha)+b(\frac{1}{2}-a)\dot{\alpha}] \quad (60)$$

It is a common practice in rotary wing analysis to identify $\dot{h}$ as a function of the normal velocity U_P, and $\dot{\alpha}$. The term $(\dot{h}+U\alpha)$ and $\dot{\alpha}$ can be expressed as [15]:

$$\dot{h} + U\alpha = U_T\theta - U_P = (\Omega\eta + \Omega R\mu \sin\psi)\theta - \left(\Omega R\lambda + \eta\dot{\beta} + \beta\Omega R\mu \cos\psi\right) \quad (61)$$

$$\dot{\alpha} = \dot{\theta} + \Omega\beta \quad (62)$$

Substitution of Eqs. (61) and (62) in Eq. (60) gives the moment expression with varying azimuth for rotary wing analysis.

The parameters of UH-60 helicopter [53, 54] are used for the calculation of airloads.

Table 2: Parameters of UH-60 Helicopter

Parameters	Value	Parameters	Value
R	8.18 m	σ	0.0826
c	0.527 m	μ	0−0.2
Ω	27 rad/s	C_{D_0}	0.0078
V_{tip}	221 m/s	C_L	0.78
airfoil	SC1095	C_T	0.005

Chapter 4

Results and Discussions

This vorticity distribution on the airfoil is shown in Fig. 4.1 for various distances of vorticity from the midchord position. The Fig. 4.1 shows that a vortex placed very close to the airfoil induces a much stronger vorticity over the chord, with a definite peak near the leading and the trailing edges.

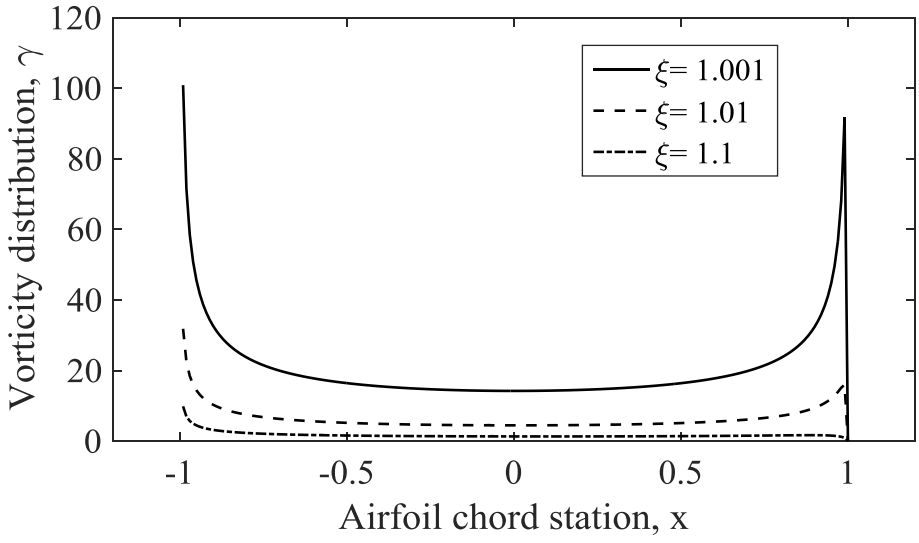

Figure 4.1: Vorticity distribution γ induced by a vortex wake at various distances ξ from the midpoint of a chord

Aerodynamic airloads− the lift, the drag, and the pitching moment of a spanwise station are computed for forward flight case considering the parameters [52−54] of the UH-60 helicopter with a varying azimuth angle from 0° to 360°. The advance ratio of UH-60 helicopter is limited to 0.21 in practice and the airloads are calculated for advance ratios of 0.1 and 0.2 for

comparison. The results for lift are obtained by using Eqs. (51)−(53) and extracting harmonics up to second harmonics and are nondimensionalized by $\pi\rho b\Omega^2R^2$. The variations of the lift at $r = 0.95, 0.75, 0.5,$ and 0.35 spanwise stations are shown in Figs. 4.2−4.5, respectively. These figures show that the advancing side of the disk, i.e., $\psi = 90°$ has the highest peak, which is the case for any flight conditions. As the advance ratio increases, the lift also increases with it. The lift is maximum near the tip and decreases gradually towards the root of the blade.

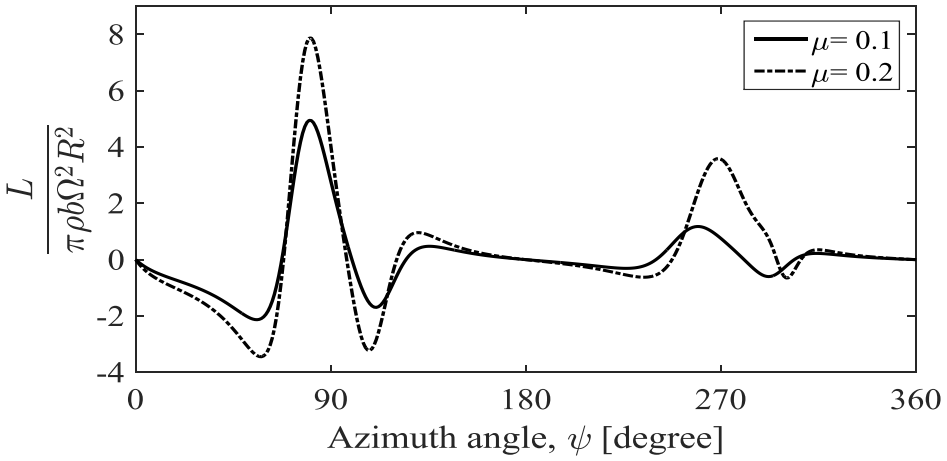

Figure 4.2: Nondimensionalized lift with varying azimuth angle of a 4-bladed rotor for advance ratios $\mu = 0.1$ and 0.2 and for the spanwise station $\eta = 0.95$ for the forward flight condition

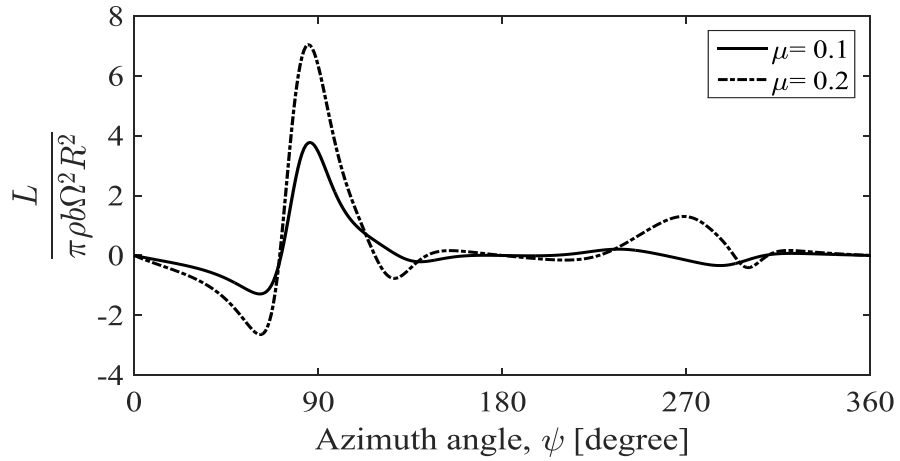

Figure 4.3: Nondimensionalized lift with varying azimuth angle of a 4-bladed rotor for advance ratios $\mu = 0.1$ and 0.2 and for the spanwise station $\eta = 0.75$ for the forward flight condition

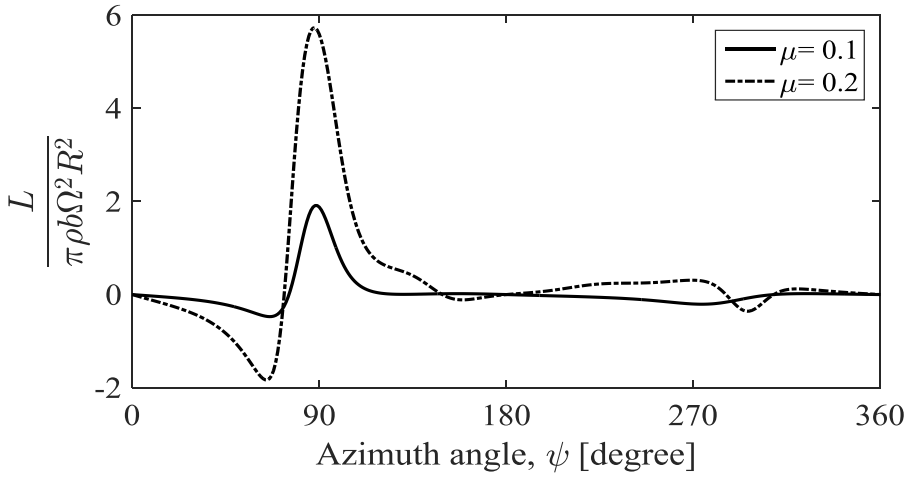

Figure 4.4: Nondimensionalized lift with varying azimuth angle of a 4-bladed rotor for advance ratios $\mu = 0.1$ and 0.2 and for the spanwise station $\eta = 0.5$ for the forward flight condition

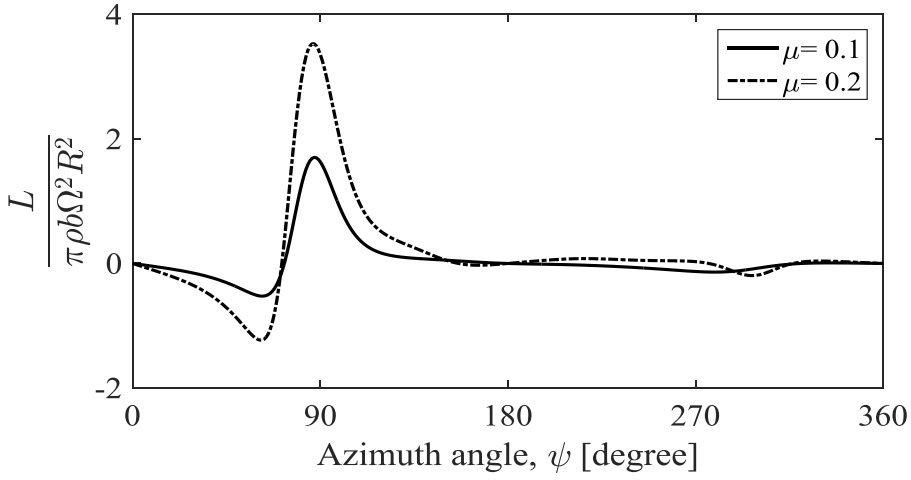

Figure 4.5: Nondimensionalized lift with varying azimuth angle of a 4-bladed rotor for advance ratios $\mu = 0.1$ and 0.2 and for the spanwise station $\eta = 0.35$ for the forward flight condition

The drag force is calculated with varying azimuth considering tangential and perpendicular air speed on the blade section for forward flight case and for a four-bladed rotor using Eq. (54). The coefficients of the blade flapping are needed for the drag calculations and are taken from Table 1. The drag forces are nondimensionalized by $\rho c\Omega^2 R^2$ and presented in Figs. 4.6−4.9. The azimuth variations of drag are shown for the advance ratios of 0.1 and 0.2 for comparison. The drag force has its highest peak at the advancing side, i.e., at $\psi = 90°$ which is similar to the results obtained for sectional lift. For advance ratio of 0.2, the drag is more at the advancing side than that of the advance ratio of 0.1.

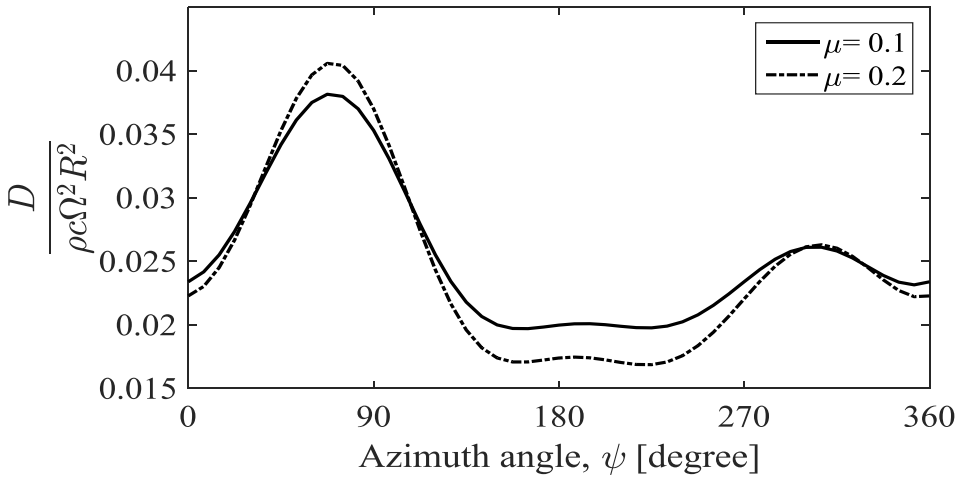

Figure 4.6: Nondimensionalized drag with varying azimuth angle of a 4-bladed rotor for advance ratios $\mu = 0.1$ and 0.2 for the spanwise station $\eta = 0.95$ for the forward flight condition

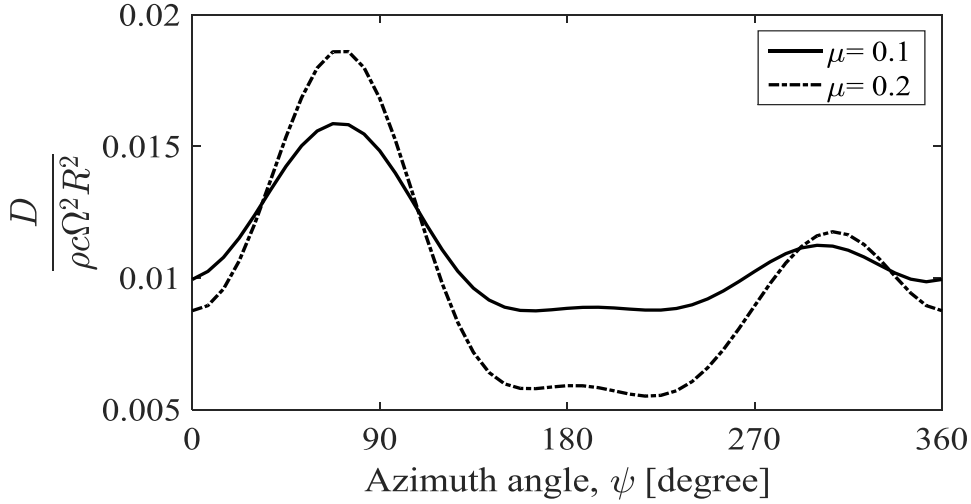

Figure 4.7: Nondimensionalized drag with varying azimuth angle of a 4-bladed rotor for advance ratios $\mu = 0.1$ and 0.2 for the spanwise station $\eta = 0.75$ for the forward flight condition

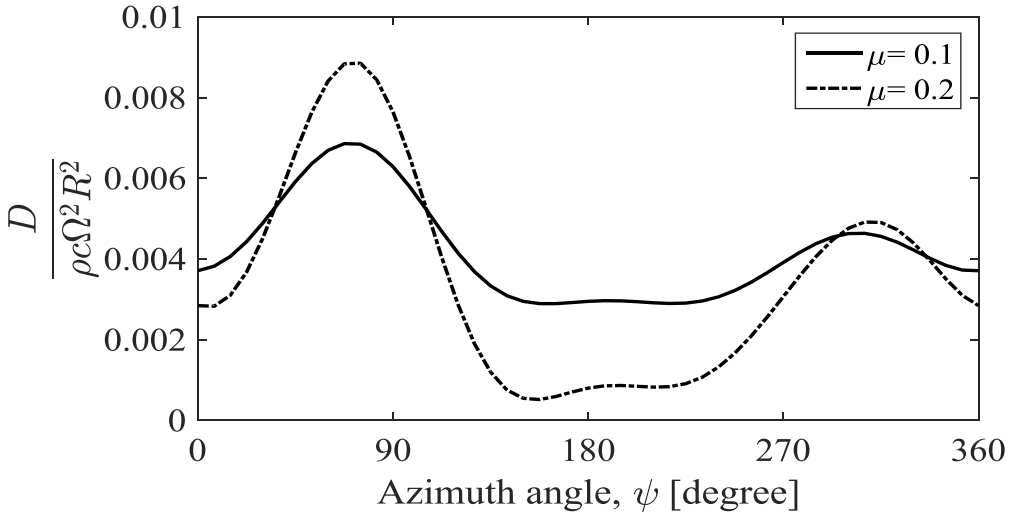

Figure 4.8: Nondimensionalized drag with varying azimuth angle of a 4-bladed rotor for advance ratios $\mu = 0.1$ and 0.2 for the spanwise station $\eta = 0.5$ for the forward flight condition

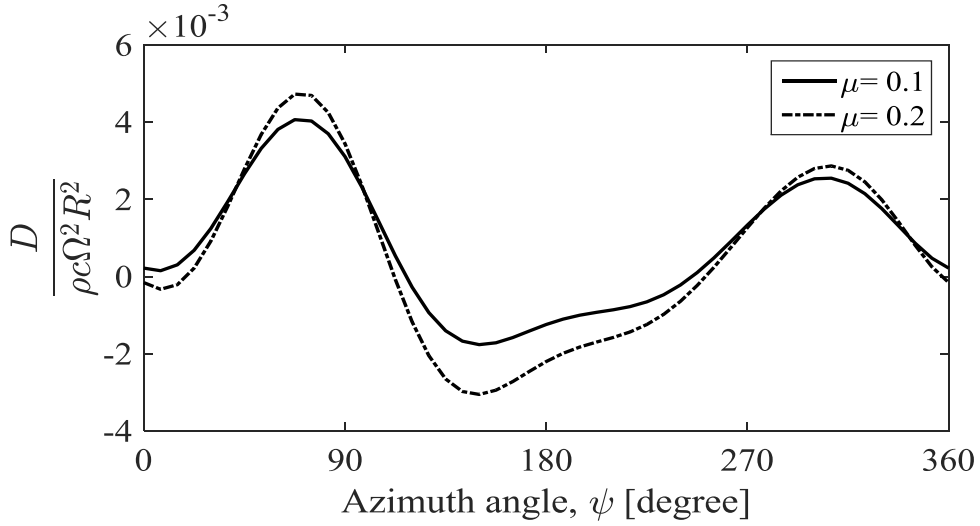

Figure 4.9: Nondimensionalized drag with varying azimuth angle of a 4-bladed rotor for advance ratios $\mu = 0.1$ and 0.2 for the spanwise station $\eta = 0.35$ for the forward flight condition

The pitching moments of the blade section are calculated with varying azimuth for the forward flight case and are shown in Figs. 4.10−4.13. The pitching moment about an axis at $x = ab$ from the midchord position is calculated using Eq. (60) and is nondimensionalized by $\pi\rho b^2$. The results are shown for advance ratios 0.1 and 0.2. At the advancing side, the pitching moment drops for both advance ratios which is the opposite case compared to the lift and drag.

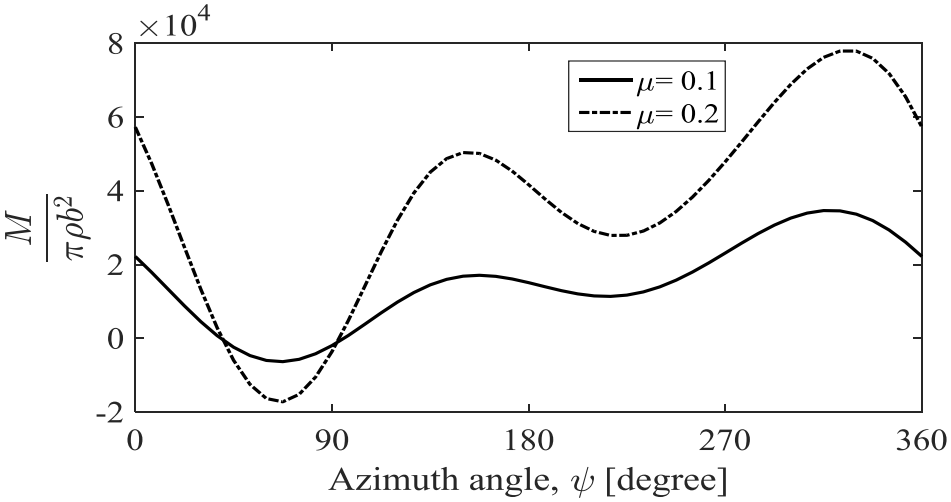

Figure 4.10: Nondimensionalized pitching moment with varying azimuth angle of a 4-bladed rotor for advance ratios $\mu = 0.1$ and 0.2 for the spanwise station $\eta = 0.95$ for the forward flight condition

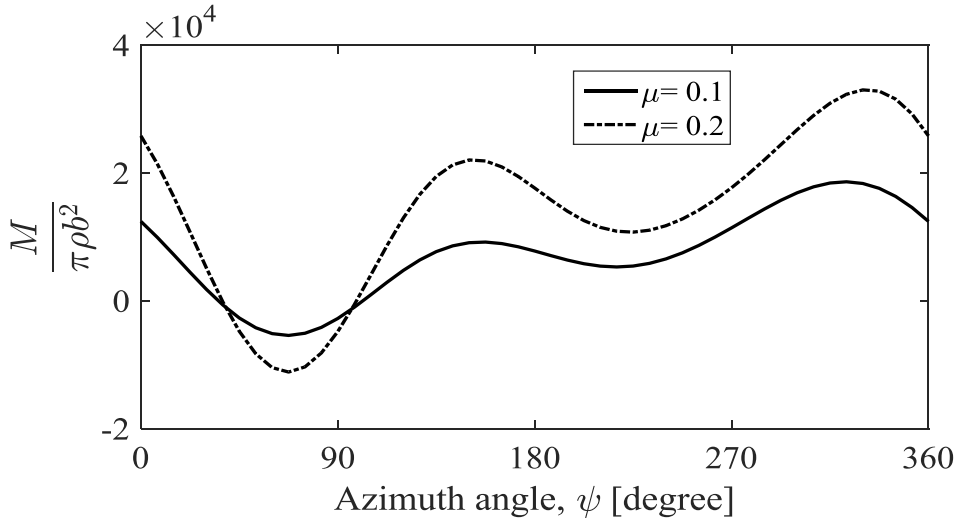

Figure 4.11: Nondimensionalized pitching moment with varying azimuth angle of a 4-bladed rotor for advance ratios $\mu = 0.1$ and 0.2 for the spanwise station $\eta = 0.75$ for the forward flight condition

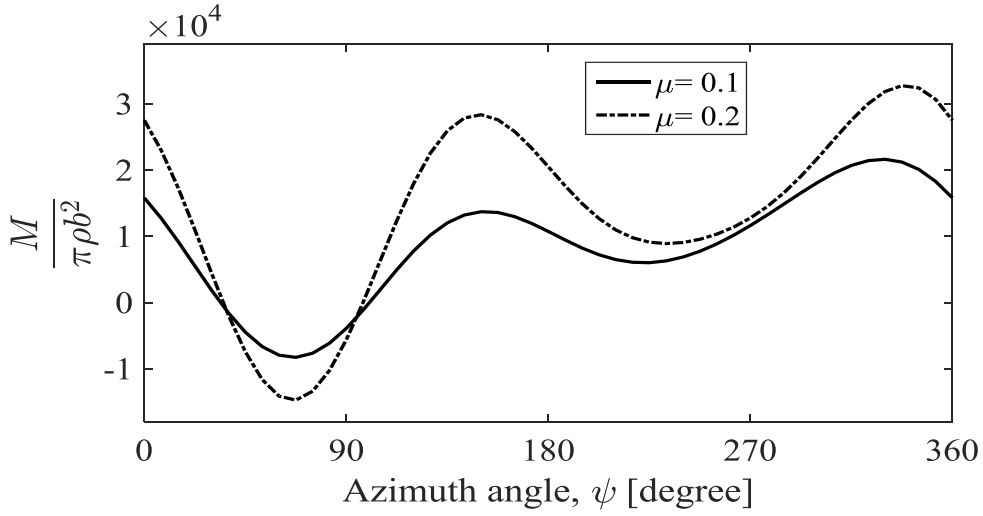

Figure 4.12: Nondimensionalized pitching moment with varying azimuth angle of a 4-bladed rotor for advance ratios $\mu = 0.1$ and 0.2 for the spanwise station $\eta = 0.5$ for the forward flight condition

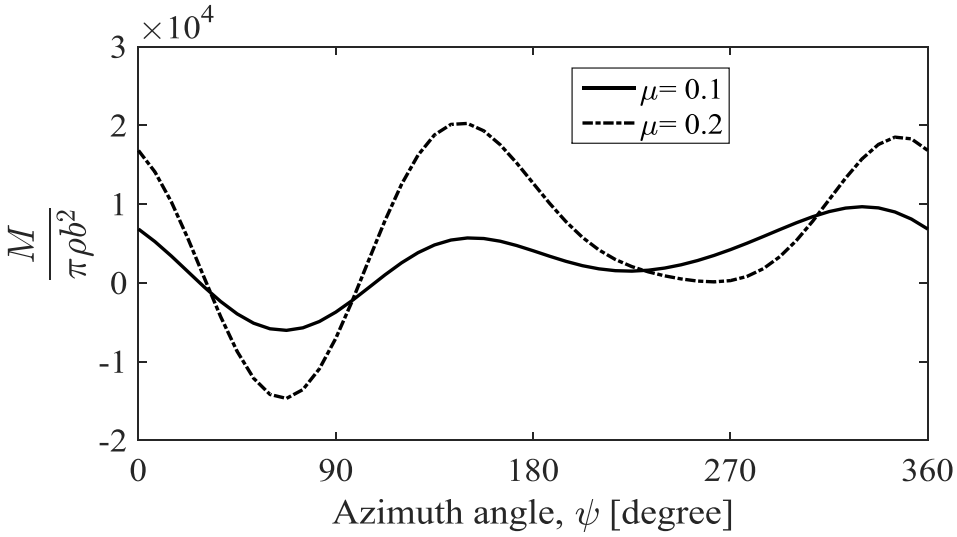

Figure 4.13: Nondimensionalized pitching moment with varying azimuth angle of a 4-bladed rotor for advance ratios $\mu = 0.1$ and 0.2 for the spanwise station $\eta = 0.5$ for the forward flight condition

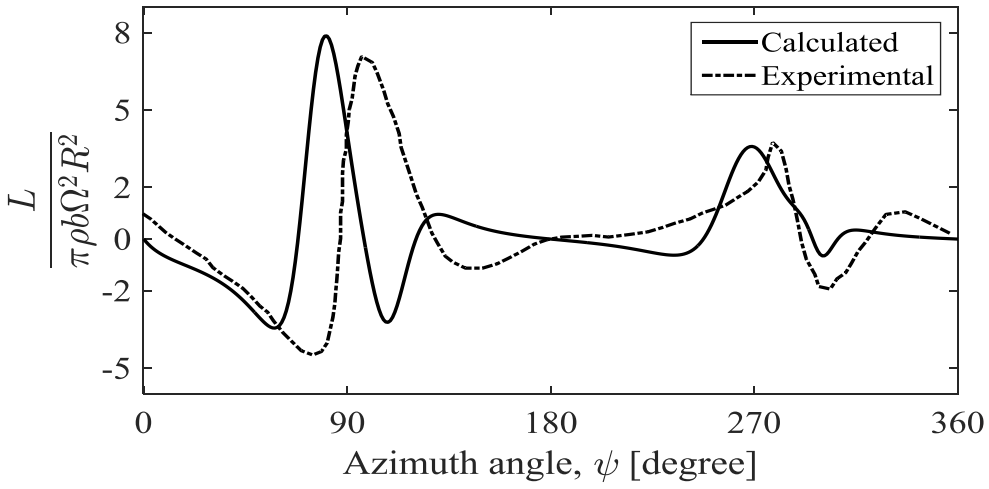

Figure 4.14: Comparison of experimental [30] and calculated lift with varying azimuth angle of a 4-bladed rotor for advance ratio $\mu = 0.2$ for the spanwise station $\eta = 0.5$ for the forward flight condition

The lower harmonics of airloads can be calculated with a reasonable accuracy by uniform inflow methods. The lift of the blade section for the forward flight case is calculated using zeroth, first, and second harmonics. For the comparison of calculated and experimental lift, NASA flight test data [30] is used. The comparison of the calculated lift with NASA flight test data [30] is shown in Fig. 4.14. The figure shows that there is a little difference as far as the ability to predict the experimental data is concerned. The calculated results for the lift show a good agreement with the experimental results.

Chapter 5

Conclusions and Recommendations

5.1 Concluding Remarks

In the thesis, the unsteady aerodynamic airloads—the lift, the drag, and the pitching moment at a particular blade section are calculated for lower harmonics. The calculated airloads are compared with the experimental flight-test data. The experimental data of blade airloads for a four-bladed rotor show good agreement with the calculated airloads. The drag and the pitching moment are also calculated at the blade section with varying azimuth. Higher harmonic variation at the blade section is not considered for the computation of airloads but it gives a good prediction of the lift variation when compared with the flight test data. Unsteady aerodynamic effects are of considerable importance for the rotary wing because of the proximity of the returning wake to the blade. These effects are simplified by treating the far wake using the lifting-line theory, and the lifting-surface theory is used for the near wake. Higher advance ratios

are not considered in this thesis for the calculation of airloads. For higher advance ratios, the consideration of only one spiral is enough instead of three for a reasonable accuracy.

The accuracy of the calculated airloads is checked by comparing with the experimental data [30]. The agreement of the calculated results with the experimental one is good and is concluded that as far as the lower harmonics are considered, the mathematical model and airloads calculation method discussed are adequate for the computation of airloads.

5.2 Recommendations and Future Work

The mathematical model discussed in this thesis is applicable to lower harmonics only. If higher harmonic airloads are to be obtained, the analytical approach discussed in this thesis has to be modified. The mathematical model presented in this thesis can be modified for higher harmonics by including the effects of vortex bursting and compressibility. Many factors contribute to higher harmonic airloads in addition to the downwash variations. In particular, the in-plane components of blade inertia loads and airloads can contribute to large pitch and flap angle variations. All these factors should be considered and the modification must be made to the mathematical model discussed in this thesis. A fluid-structure interaction model can be developed for rotor blade system and compared to the results obtained for modified mathematical model.

The best approach is to use modern panel codes or CFD solver to compute the higher harmonic airloads. The solutions of Reynolds-averaged Navier-Stokes (RANS) equations offer significant improvements in the calculation of blade airloads, compared to methods based on lifting-line theory. There are some commercially available software like CAMRAD II to calculate the airloads for higher harmonics.

REFERENCES

[1] Miller, R.H., 1964, "Rotor Blade Harmonic Air Loading," *AIAA Journal*, **2** (7) 1254−1269.

[2] Johnson, W., 1971, "A Lifting-Surface Solution for Vortex-Induced Airloads," *AIAA journal*, **9** (4) 689−695.

[3] Anderson, J., "Fundamental of Aerodynamics," McGraw-Hill, Boston.

[4] Theodorsen, T., 1949, "General Theory of Aerodynamic Instability and the Mechanism of Flutter," National Advisory Committee for Aeronautics, TR 496.

[5] Karman, V., Sears, W.R., 1938, "Airfoil Theory for Non-Uniform Motion," *Journal of the Aeronautical Sciences*, **5** (10) 379−390.

[6] Isaacs, R., 1945, "Airfoil Theory for Flows of Variable Velocity," *Journal of the Aeronautical Sciences*, **12** (1) 113−117.

[7] Isaacs, R., 1946, "Airfoil Theory for Rotary Wing Aircraft," *Journal of the Aeronautical Sciences*, **13** (4) 218−220.

[8] Loewy, R., 1957, "A Two-Dimensional Approximation to the Unsteady Aerodynamics of Rotary Wings," *Journal of the Aeronautical Sciences*, **24** (2) 81−92.

[9] Peters, D., 2008, "Two-Dimensional Incompressible Unsteady Airfoil Theory-An Overview," *Journal of Fluids and Structures*, **24** (3) 295−312.

[10] Liu, T., 2015, "Unsteady Thin-Airfoil Theory Revisited: Application of a Simple Lift Formula," *AIAA Journal*, **53** (6) 1492−1502.

[11] Giesing, J.P., 1968, "Nonlinear Two-Dimensional Unsteady Potential Flow with Lift," *Journal of Aircraft*, **5** (2) 135−143.

[12] Srinivasan, G., McCroskey, W., Baeder, J., 1985, "Aerodynamics of Two-Dimensional Blade-Vortex Interaction," 18th Fluid Dynamics and Plasma Dynamics and Lasers Conference.

[13] Colin, O., 1973, "Unsteady Thin-Airfoil Theory for Subsonic Flow," *AIAA Journal*, **11** (2) 205−209.

[14] Basu, B.C., Hancock, G.J., 1978, "The Unsteady Motion of a Two-Dimensional Aerofoil in Incompressible Inviscid Flow," *Journal of Fluid Mechanics*, **87** (1) 159−178.

[15] Johnson, W., 1980, "Application of Unsteady Airfoil Theory to Rotary Wings," *Journal of Aircraft*, **17** 285−286.

[16] Johnson, W., 2013, "Rotorcraft Aeromechanics," Cambridge University Press.

[17] Phillips, W.F., Snyder, D.O., 2000, "Modern Adaptation of Prandtl's Lifting Line Theory," *Journal of Aircraft*, **37** (4) 662−670.

[18] Jones, J.P., 1965, "An Extended Lifting Line Theory for the Loads on a Rotor Blade in the Vicinity of a Vortex," Technical Report 123−3, MIT Aeroelastic and Structures Research Laboratory.

[19] Ashley, H., Landhal, M.T., Windall, S., 1965, "New Directions in Lifting-Surface Theory," *AIAA Journal*, **3**(1) 3−16.

[20] Landhal, M.T., Stark, V.J.E., 1968, "Numerical Lifting-Surface Theory−Problems and Progress," *AIAA Journal*, **6** (11) 2049−2060.

[21] Tai, H., Runyan, H.L., 1985, "Lifting Surface Theory for a Helicopter Rotor in Forward Flight," NASA Langley Research Center, Hampton, Virginia.

[22] Kussner, H. G., 1941, "General Airfoil Theory," National Advisory Committee for Aeronautics, TM 979.

[23] Johnson, W., 1970, "A Lifting Surface Solution for Vortex Induced Airloads and its Application to Rotary Wing Airload calculation," PhD Thesis, MIT.

[24] Watkins, C.E., Runyan, H.C., Woolston, D.S., 1955, "On the Kernel Function of the Integral Equation Relating the Lift and Downwash Distributions of Oscillating Finite Wings in Subsonic Flow," NACA Technical Report 1234.

[25] Watkins, C.E., Woolston, D.S., Cunningham, H.J., 1959, "A Systematic Kernel Function Procedure for Determining Aerodynamic Forces on Oscillating or Steady Finite Wings at Subsonic Speeds," NASA Technical Report R−48.

[26] Drees, J.M., 1949, "A Theory of Airflow through Rotors and its Application to Some Harmonic Problems," *The Journal of the Helicopter Association of Great Britain*, **3** (2) 79−104.

[27] Miller, R.H., 1963, "Theoretical Determination of Rotor Blade Harmonic Airloads," Technical Report 107−2, MIT.

[28] Miller, R.H., 1962, "On the Computation of Airloads Acting on Rotor Blades in Forward Flight," *Journal of the American Helicopter Society*, **7** (2) 56−66.

[29] Ghareeb, N., 1964, "Programs for Machine Computation of Rotor Blade Downwash," Part 1, ASRL Report No. 107−1, MIT.

[30] Scully, M.P., 1965, "Approximate Solutions for Computing Helicopter Harmonic Airloads," Part 1, ASRL Report No. 123−2, MIT.

[31] Scully, M.P., 1975, "Computation of Helicopter Rotor Wake Geometry and its Influence on Rotor Harmonic Airloads," PhD Thesis, Department of Aeronautics and Astronautics, MIT.

[32] Widnall, S.E., 1972, "The Stability of a Helical Vortex Filament," *Journal of Fluid Mechanics*, **54** (4) 641−663.

[33] Scully, M.P., 1967, "A Method of Computing Helicopter Vortex Wake Distortion," MIT Aeroelastic and Structures Research Laboratory, ASRL TR 138−1.

[34] Landgrebe, A.J., 1969, "An Analytical Method for Predicting Rotor Wake Geometry," *Journal of the American Helicopter Society*, **14** (4) 20−32.

[35] Scully, M.P., 1965, "Approximate Solutions for Computing Helicopter Harmonic Airloads," MIT Aeroelastic and Structures Research Laboratory, ASRL TR 123−2.

[36] Madden, P.A., 1967, "Angle-of-Attack Distribution of a High Speed Helicopter," *Journal of the American Helicopter Society*, **12** (2) 41−49.

[37] Kartz, J., Maskew, B., 1988, "Unsteady Low-speed Aerodynamic Model for Complete Aircraft Configurations," *Journal of Aircraft*, **25** (4) 302-310.

[38] Mello, O., Rand, O., 1991, "Unsteady, Frequency-Domain Analysis of Helicopter Non-Rotating Lifting Surfaces," *Journal of the American Helicopter Society*, **36** (2) 70−81.

[39] Kocurek, J.D., Berkovitz, L.F., 1982, "Velocity Coupling: A New Concept for Hover and Axial Flow Wake Analysis and Design," CP-334, Prediction of Loads on Rotorcraft, AGARD.

[40] Johnson, W., 1989, "Calculation of Blade-Vortex Interaction Airloads on Helicopter Rotors," *Journal of Aircraft*, **26** 470−475.

[41] Bengin, A., Mitrovic, C., Cvetkovic, D., 2008, "Improved Solution Approach for Aerodynamics Loads of Helicopter Rotor Blade in Forward Flight," *Journal of Mechanical Engineering*, **54** (3) 170−178.

[42] Daughaday, H., Piziali, R.A., 1967, "An Improved Computation Model for Predicting the Unsteady Aerodynamic Loads of Rotor Blades," *Journal of the American Helicopter Society*, **12** (2) 3−10.

[43] Zioutis, C.K., Spyropoulos, A.I., 2010, "Influence of Helicopter Rotor Wake Modeling on Blade Airload Prediction," *International Journal of Engineering*, **3** (6) 521−535.

[44] Crispin, Y., 1982, "Unsteady Rotor Aerodynamics Using a Vortex Panel Method," 9th Atmospheric Flight Mechanics Conference, San Diego, California.

[45] Leishman, J.G., 2000, "Principles of Helicopter Aerodynamics," Cambridge University Press.

[46] Leishman, J.G., Martin, G.L., 2002, "Challenges in Modelling the Unsteady Aerodynamics of Wind Turbines," ASME Wind Energy Symposium, **5** 85−132.

[47] Ilie, M., Smith, S.L., 2009, "Critical Aerodynamic Aspects of Helicopter Blade-Vortex Interaction: A Numerical Study Using Large-Eddy Simulation," 27th AIAA Applied Aerodynamics Conference, San Antonio, Texas.

[48] Cottet, G.H., Koumoutsakos, P.D., 2000, "Vortex Methods: Theory and Practice," Cambridge University Press.

[49] Johnson, W., 2013, "Helicopter Theory," Dover Publications, New York.

[50] Bisplinghoff, R.L., Ashley, H., Halfman, R., 1955, "Aeroelasticity," Addison and Wesley.

[51] Glauert, H., 1959, "The Elements of Aerofoil and Airscrew Theory," Cambridge University Press.

[52] Kathryn, B.H., "A Mathematical Model of the UH-60 Helicopter," NASA TM-85890, Ames Research Center, Moffett Field, California.

[53] William, G.B., "Aerodynamic Characteristics of SC1095 and SC1094 R8 Airfoils," NASA TP-212265, Ames Research Center, Moffett Field, California.

[54] Patrick, M.S., Hyeonsoo, Y., Norman, T.R., 2002, "Rotor Performance of a UH-60 Rotor Syatem in the NASA Ames 80-by 120-foot Wind Tunnel," 58th Annual Forum of the American Helicopter Society, Montreal, Canada.

[55] Kheim, V.T., 2016, "Modeling Aerodynamics for Comprehensive Analysis of Helicopter Rotors," 42nd European Rotorcraft Forum, Lille, France.

[56] Biedron, R.T., 2011, "Computation of UH-60A Airloads using CFD/CSD coupling on Unstructured Meshes," 67th Annual Forum of the American Helicopter Society, Virginia Beach, Virginia.

[57] Sarker, P., Theodore, C.R., Chakravarty, U.K., 2016, "Vibration Analysis of a Composite Helicopter Rotor Blade at Hovering Condition," ASME International Mechanical Engineering Congress and Exposition, Phoenix, Arizona.

VITA

The author was born in the city of Dhaka, Bangladesh and passed his early school and college years in Faujdarhat Cadet College in Chittagong city. He obtained his Bachelor's degree in Naval Architecture and Marine Engineering in 2014 at Bangladesh University of Engineering and Technology (BUET). After graduation, he joined Dockyard and Engineering Works Ltd., Bangladesh Navy and served there as an Assistant Engineer until June 2016. In the Fall 2016, he joined the University of New Orleans to pursue his Master of Science in Engineering with concentration in Mechanical Engineering degree.